Identification of Polyethylene Glycol-Resistant Macrophages on Stealth Imaging *in Vitro* Using Fluorescent Organosilica Nanoparticles

Michihiro Nakamura,[*,†] Koichiro Hayashi,[†,¶] Mutsuki Nakano,[†,‡] Takafumi Kanadani,[†,‡] Kazue Miyamoto,[†,‡] Toshinari Kori,[⊥] and Kazuki Horikawa[§]

[†]Department of Anatomy and Cell Biology, The University of Tokushima Graduate School of Medical Sciences, 3-18-15 Kuramoto, Tokushima 770-8503, Japan, [‡]Student Lab, The University of Tokushima Faculty of Medicine, 3-18-15 Kuramoto, Tokushima 770-8503, Japan, [⊥]Tokushima Prefectural Industrial Technology Center, 11-2 Nishibari, Saigacho, Tokushima 770—8021, Japan, and [§]Division of Bioimaging, Institute of Health Biosciences, The University of Tokushima Graduate School, 3-18-15 Kuramoto, Tokushima 770-8503, Japan. [¶]Present address for K. Hayashi: Division of Green Materials, EcoTopia Science Institute, Nagoya University, Furo-cho, Chikusa-ku, Nagoya 464-8603, Japan.

ABSTRACT An *in vitro* imaging system to evaluate the stealth function of nanoparticles against mouse macrophages was established using fluorescent organosilica nanoparticles. Surface-functionalized organosilica nanoparticles with polyethylene glycol (PEG) were prepared by a one-step process, resulting in a brush-type PEG layer. A simultaneous dual-particle administration approach enabled us to evaluate the stealth function of nanoparticles with respect to single cells using time-lapse fluorescent microscopic imaging and flow cytometry analyses. Single-cell imaging and analysis revealed various patterns and kinetics of bare and PEGylated nanoparticle uptake. The PEGylated nanoparticles revealed a stealth function against most macrophages (PEG-sensitive macrophages); however, a stealth function against certain macrophages (PEG-insensitive macrophages) was not observed. We identified and characterized the PEG-resistant macrophages that could take up PEGylated nanoparticles at the same level as bare nanoparticles.

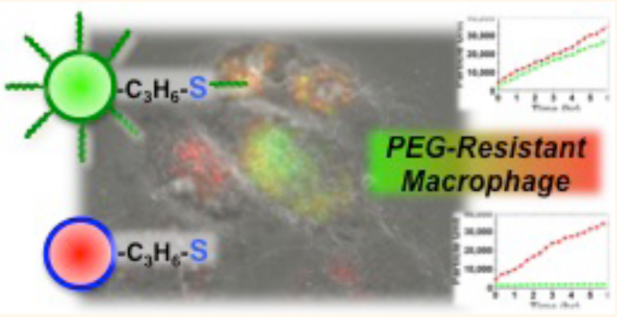

KEYWORDS: stealth nanoparticles · single-cell analysis · polyethylene glycol · macrophages · accelerated blood clearance

Recent advances in the development of multifunctional nanoparticles have led to innovations in the field of nanomedicine.[1−12] Multifunctional nanoparticles that have strong and specific signals for various imaging modalities, bind targets with high affinity and specificity, and are adaptable for the delivery of specific pharmacological agents to targets of interest would enable the establishment of advanced medicines that could cure patients without any distress. Upon systemic administration, the pharmacokinetics of nanoparticles are different from those of small molecules. In tumor tissues, nanoparticles can extravasate from the leaky tumor vasculature to a higher degree than from healthy tissue and remain in the area by the enhanced permeability and retention (EPR) effect.[13−15] However, there are problems that must be solved to fully realize such successful nanomedicines. Many studies have reported that intravenously administered nanoparticles are cleared from the blood by the reticuloendothelial system (RES) within minutes. The removal of nanoparticles is initiated by interactions between the administered nanoparticles and phagocytic cells (such as macrophages) in the blood and tissues. Nanoparticles that are intended for systemic administration are functionalized on the surface with stealth molecules such as polyethylene glycol (PEG). The circulation half-life of these stealth nanoparticles can be extended because of a reduction of macrophage uptake.[16] However, an accelerated blood clearance (ABC) of surface-functionalized nanoparticles has been reported after the second nanoparticle administration.[17−21] The mechanism of the ABC phenomenon is

* Address correspondence to michy@basic.med.tokushima-u.ac.jp, michi.nakamura@tokushima-u.ac.jp.

Received for review April 29, 2014 and accepted January 28, 2015.

Published online January 28, 2015
10.1021/nn502319r

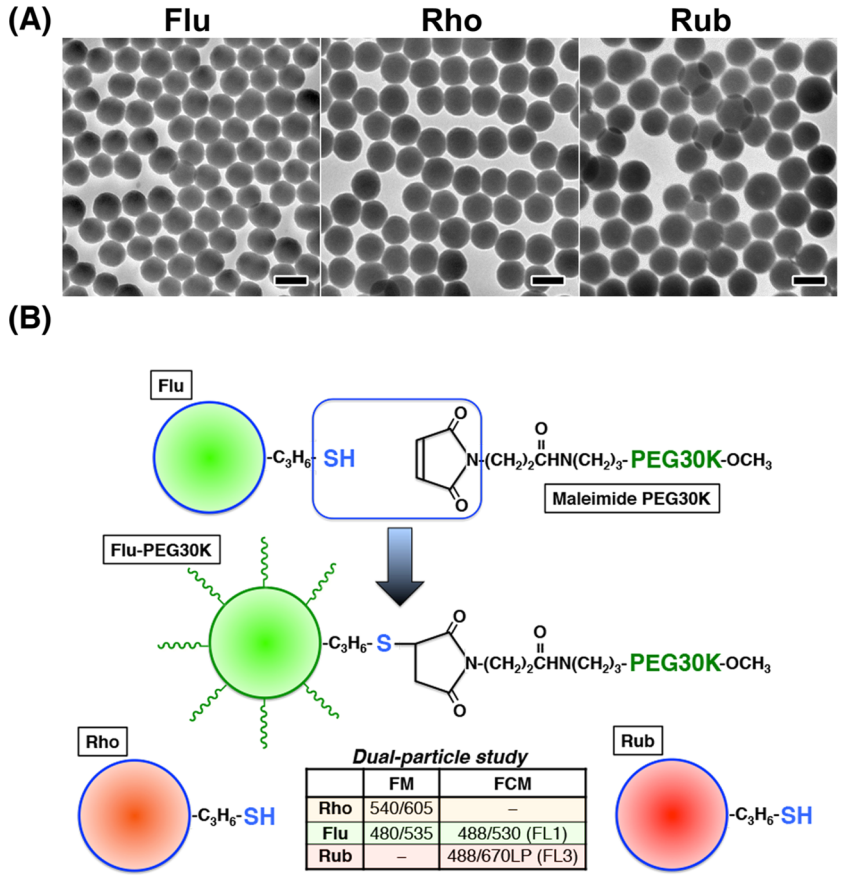

Figure 1. Characterization of fluorescent organosilica nanoparticles for the dual-particle administration study. (A) Transmission electron micrographs of fluorescent organosilica nanoparticles containing fluorescein isothiocyanate (Flu), rhodamine B (Rho), or trisdichlororuthenium(II) hexahydrate (Rub). The scale bars represent 100 nm. (B) Reaction scheme for the surface functionalization of Flu with methoxy-PEG-maleimide and the table of fluorescent conditions for the dual particle administration study on fluorescent microscopy (FM) and flow cytometry (FCM).

not fully understood but may be mediated by the low-specificity, anti-PEG immunoglobulin (Ig) M antibody (anti-PEG IgM).[21−23] Understanding and controlling the interactions between stealth nanoparticles and immune cells, especially macrophages, are therefore very important for the development of effective nanomedicines.

In this paper, we demonstrated a novel *in vitro* imaging system to visualize the stealth effect of nanoparticles against mouse peritoneal macrophages using fluorescent organosilica nanoparticles. Organosilica nanoparticles are novel nanomaterials that are prepared from a single organosilicate coupling agent, such as 3-mercaptopropyltrimethoxysilane (MPMS).[24−31] Organosilica nanoparticles are structurally and functionally different from typical inorganosilica particles prepared from tetraethoxyorthosilicate (TEOS). Organosilica nanoparticles contain an organic residue with the same number of Si atoms and can be internally functionalized with various fluorescent dyes and fluorescent nanomaterials using an organic residue. Fluorescent organosilica nanoparticles are useful for various fluorescence imaging techniques such as *in vivo* imaging,[29,30] cell labeling,[26,28,29,32,33] real-time or time-lapse fluorescent imaging with single cell analysis,[28,34] molecular tracing,[29] and multimodal imaging.[30] The functional groups on the surface of organosilica nanoparticles are very useful for surface functionalization, and the preparation of PEG attached (PEGylated) nanoparticles is straightforward. To evaluate the stealth effect of PEG, we performed time-lapse fluorescence microscopic imaging and flow cytometry using macrophages that were simultaneously treated with PEGylated nanoparticles and bare nanoparticles. The PEGylated nanoparticles demonstrated a stealth effect against mouse peritoneal macrophages. We identified macrophages that could take up PEGylated nanoparticles to the same extent as bare nanoparticles. We discuss the importance of stealth imaging *in vitro* and the potential of PEG-resistant macrophages for the development of drug delivery systems and innovative nanomedicine.

RESULTS AND DISCUSSION

Surface Functionalization with PEG and Characterization of Fluorescent Organosilica Nanoparticles. Three types of fluorescent organosilica nanoparticles containing fluorescein (Flu), rhodamine B (Rho), or Rubpy (Rub) were prepared and observed on transmission electron microscopy (TEM). TEM revealed that these three nanoparticles had

TABLE 1. Characterization of Fluorescent Organosilica Nanoparticles

fluorescent organosilica nanoparticles	EM avg diameter (nm)	EM CV (%)	ζ potential (mV)
Flu	87.1	7.6	−57.1
Flu-PEG30K			−50.9
Flu-PEG12K			−33.9
Rho	99.1	6.8	−53.8
Rub	105.3	9.7	−41.8

a spherical shape, narrow size distribution, and good dispersions (Figure 1A). The average diameters and coefficients of variation (CVs) of the particles derived from TEM are summarized in Table 1. The diameter and percentage of the CVs of Flu, Rho, and Rub were approximately 100 nm and 8%. The Flu were PEGylated using methoxy-PEG-maleimide with a molecular weight of 30 KDa in a one-step process (Flu-PEG30K) (Figure 1B). However, we performed dynamic light scattering (DLS) (Supporting Information, Figure S1 and Table S1), and the results indicated that DLS analysis could not be quite appropriate to evaluate the sizes of these particles including additionally prepared Flu-PEG12K due to the property of organosilica particles as reported previously.[35]

To evaluate the density of PEGs on particle, we performed thermal gravimetric analysis (TGA) of Flu, Flu-PEG12K, and Flu-PEG30K. The initial weight loss under 200 °C is due to the desorption of water molecules from the surface of the particle. The remaining weights were 60.4%, 57.9%, and 55.3% at 200−800 °C in flowing argon for Flu, Flu-PEG12K, and Flu-PEG30K, respectively (Figure 2 and Table 2). The calculated PEG densities of Flu-PEG12K and Flu-PEG30K were 0.031 and 0.032 PEG/nm^2, respectively (Table 2).

The PEG surface layer is often described as either a mushroom- or brush-type layer. When the surface PEG density is relatively low, a mushroom-like structure is formed to maximize surface coverage.[36] As the PEG density increases, the PEG chains extend to avoid overlapping with other PEG molecules, resulting in a brush-type structure.[36,37] The distance between the PEGs of Flu-PEG30K was 31.6 nm, smaller than the Flory radius of PEG30K (35 nm). These results indicated that Flu-PEG30K might adopt a brush-type structure and have a more densely PEGylated surface than Flu-PEG12K. However, the DLS analyses were not useful for organosilica particles, and the PEG weights were not so high upon TGA analysis. The determination of the PEG layer type on organosilica particles should be discrete. Further studies were required for the evaluation and determination of the PEG layer type on organosilica particles.

The ζ potentials of Flu, Flu-PEG30K, Rho, and Rub were similar to each other, and the ζ potential of Flu-PEG30K was slightly less negative than that of Flu (Table 1). However, the ζ potential of Flu-PEG12K

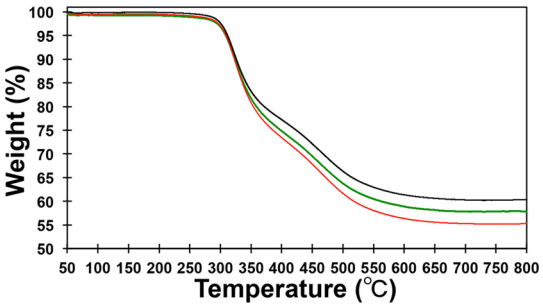

Figure 2. Thermal gravimetric analysis of PEGylated nanoparticles. The data for Flu (black), Flu-PEG12K (green), and Flu-PEG30K (red) were obtained in flowing argon.

TABLE 2. Thermal Gravimetric Analyses and PEG Densities of PEGylated Nanoparticles[a]

	Flu	Flu-PEG12K	Flu-PEG30K
wt at 200 °C (%)	99.94	99.24	99.57
wt at 800 °C (%)	60.40	57.88	55.30
organic part (%)	39.54	41.36	44.27
PEG part (%)		1.82	4.73
PEG weight (g)/particle		1.46×10^{-17}	3.77×10^{-17}
PEG number/particle		732.48	757.59
PEG density (PEG/nm2)		0.031	0.032

[a] The weight of one particle (7.95×10^{-13} mg) was calculated from the volume of one particle as follows: 4π (r = 87.1 (nm))^3/3 × 2.3 (specific gravity).

was lower than −35 mV and similar to inorganosilica prepared from TEOS and surface-modified thiol organosilica nanoparticles with rhodamine red−maleimide as reported previously by us.[24] The ζ potentials of Flu-PEG12K and Flu-PEG30K were different, but TGA analysis of Flu-PEG12K and Flu-PEG30K revealed similar PEG densities. Because the distance value between the PEGs of Flu-PEG12K was higher than the Flory radius of Flu-PEG12K and the CV of the diameter of Flu-PEG12K based on DLS was higher than that of Flu-PEG30K, it is possible that the PEG12K on Flu-PEG12K had a higher flexibility. The flexible PEG12K may cover the thiol group as well as the silanol group on the surface of the particles and influence the ζ potential. The PEG density and ζ potential value of Flu-PEG30K indicated that the reaction between the methoxy-PEG-maleimide and thiol residues on Flu was partial and that there may be thiol residues that do not react to it. As described, Flu-PEG30K showed stealth effects without much loss of functional thiol residues on the surface of the particles. Further functionalizations of the particles are possible. The ζ potential of Flu-PEG30K was not substantially different from those of Rho and Rub. Both Rho and Rub were suitable as control bare nanoparticles for simultaneous dual-particle administration studies using time-lapse fluorescent imaging (TLFI) and flow cytometry analysis (FCM).

Time-Lapse Fluorescent Microscopic Imaging and Single-Cell Analysis Using Fluorescent Organosilica Nanoparticles Surface Functionalized with PEG. We performed TLFI microscopy

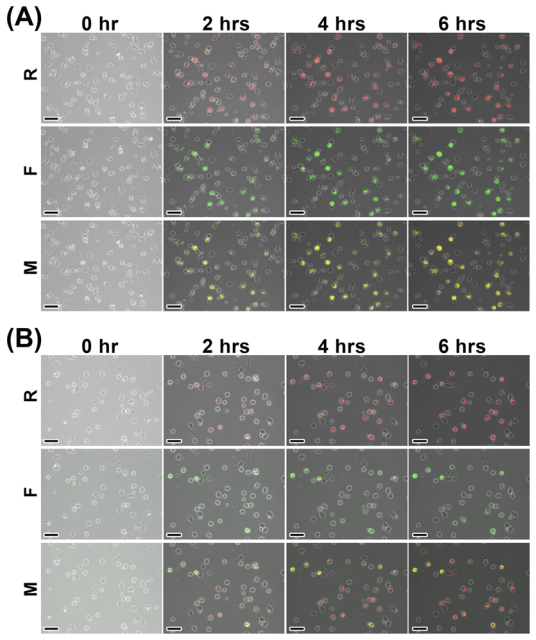

Figure 3. Time−lapse imaging of the dual-particle administration study of macrophage uptake of fluorescent organosilica nanoparticles surface functionalized with PEG. The macrophages were incubated with a mixture of Flu and Rho (A) or with a mixture of Flu-PEG30K and Rho (B). Fluorescence images of Rub (R), Flu or Flu-PEG30K (F), and merged images (M) are shown from 0 to 6 h. The scale bars represent 40 μm.

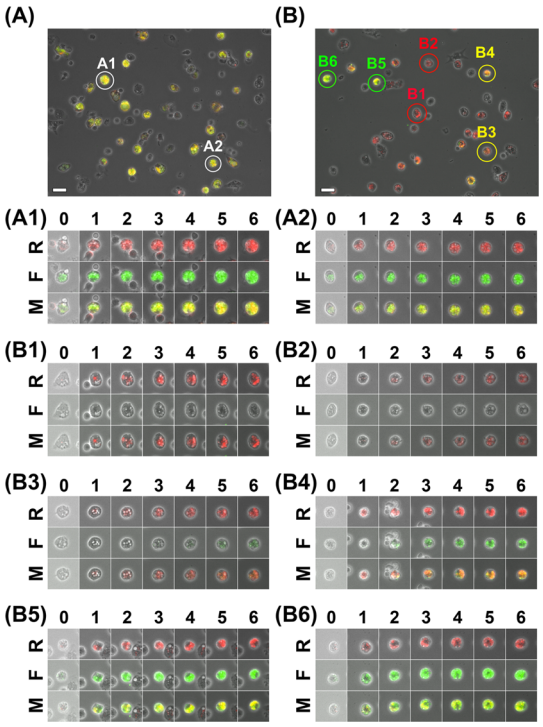

Figure 4. Single-cell dual-particle images showing macrophage uptake of fluorescent organosilica nanoparticles surface functionalized with PEG. The macrophages were incubated with a mixture of Flu and Rho (A) or with a mixture of Flu-PEG30K and Rho (B). The fluorescence images of Rub (R), Flu or Flu-PEG30K (F), and merged images (M) of single cells are shown from 0 to 6 h. The scale bars represent 40 μm. Cells A1 and A2 showed similar uptake of Flu and Rho. Cells B1 and B2 showed uptake of Rho and almost no uptake of Flu-PEG30K. Cells B3 and B4 showed uptake of Rho and a lower uptake of Flu-PEG30K. Cells B5 and B6 showed a similar uptake of Flu, Rho, and Flu-PEG30K.

to visualize the PEG effect against mouse peritoneal macrophages using Flu-PEG30K. We previously reported that the uptake level and kinetics of each macrophage were heterogeneous.[34] We used a simultaneous dual-particle administration study using two types of particles with different internal fluorescence and surface structure to directly compare the particles in single cells *in vitro*. The macrophages were incubated with 10 μg/mL of Flu and Rho or with Flu-PEG30K and Rho for 6 h. As shown in Figure 3A, both bare Flu and Rho were taken up similarly (Supporting Information, movie 1). However, the uptakes of Flu-PEG30K and Rho into the cells (Figure 3B and Supporting Information, movie 2) were different. Many cells showed uptake of only Rho, but some cells showed uptake of both Rho and Flu-PEG30K. Figure 4 shows enlarged views of the pictures at 6 h of Figure 3. As shown in Figure 4A, the cells (Figure 4A1,A2) containing nanoparticles showed both Flu and Rho fluorescence. The macrophages incubated with Flu-PEG30K and Rho showed various patterns. Many cells showed only Rho fluorescence (B1 and B2), and some cells showed fluorescence of both Flu and Rho (B3−B6). Cells B3 and B4 had uptake of Rho and Flu-PEG30K at lower levels. Cells B5 and B6 showed similar uptake levels of Flu-PEG30K and Rho.

As shown in Figure 5, we then performed single-cell analyses using particle units (PU) to quantitatively compare the differences in uptake. The PU was calculated as described previously[34] and may indicate the number of particles in a single cell. Cells A1 and A2 took up the two types of nanoparticles in similar amounts. A quantitative difference in the uptake kinetics between these cells was detected after approximately 2 h. Cell A1 showed a greater linear uptake of Rho and later showed a slow uptake of Flu; the PU of Rho was approximately 70000 at 6 h. Cell A2 showed the reverse pattern of the A1 cell, with a moderate uptake. It is possible that cells A1 and A2 distinguish the slight difference in the surface structure of particles due to the difference of the fluorescent dye between Flu and Rho. These results and the heterogeneity of each macrophage uptake of fluorescent organosilica nanoparticles may indicate an existence of selective uptake of each macrophage against the slight difference of particles. Further studies are required to demonstrate and characterize these selective uptakes of each macrophage and are under investigation. The single-cell analyses of macrophages incubated with Flu-PEG30K and Rho also revealed different patterns. Cells B1 and B2 showed a linear uptake of Rho but almost no uptake of Flu-PEG30K. These results demonstrated that Flu-PEG30K had a stealth effect. The heterogeneity of

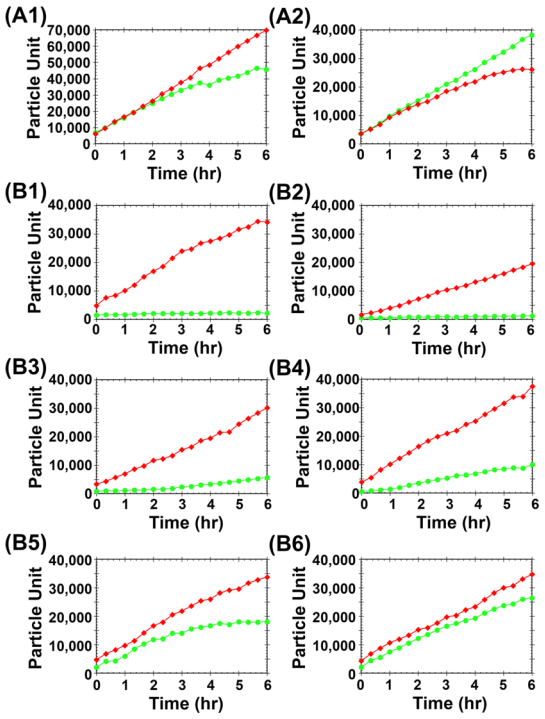

Figure 5. Quantitative single-cell dual-particle analyses of macrophage uptake of fluorescent organosilica nanoparticles surface functionalized with PEG. The macrophages were incubated with a mixture of Flu and Rho (A) or with a mixture of Flu-PEG30K and Rho (B). Cell A1 showed a greater linear uptake of Rho and a later slow uptake of Flu. Cell A2 showed the reverse pattern of cell A1. Cells B1 and B2 showed a linear uptake of Rho and almost no uptake of Flu-PEG30K. Cells B3 and B4 showed a linear uptake of Rho and a slow uptake of Flu-PEG30K with lag phases of approximately 2 h and less than 1 h, respectively. Cell B5 showed a later slow uptake of Flu-PEG30K. Cell B6 showed a linear uptake of Flu-PEG30K and had 77.7% of PU compared with Rho.

the PEGylated particles was estimated on the basis of the greater CV of their measured diameter. It is possible that a small proportion of particles with less PEGylation exists and contributed a small increase of the PU of Flu-PEG30K in these cells. Cells B3 and B4 showed a linear uptake of Rho with a lag phase and a slow uptake of Flu-PEG30K. Cells B3 and B4 showed increased uptake after approximately 2 h, and within 1 h, these cells showed 18.8% and 26.7%, respectively, of the PU of Flu-PEG30K compared to the values for Rho at 6 h. Cells B5 and B6 showed 53.4% and 77.7% of the PU of Flu-PEG30K compared to the values for Rho, respectively. Cells B5 and B6 showed a later slow uptake and a linear uptake of Flu-PEG30K, respectively.

We could perform TLFI and single-cell analysis using fluorescent organosilica nanoparticles successfully. Fluorescent nanocrystals, often referred to as quantum dots (QDs), have been intensively used for fluorescence imaging. QDs have several advantages such as broad excitation spectra, size-tunable fluorescence properties, and long fluorescence emission times.[38] However, it has been reported that the fluorescent intensity of QDs in endosome can be changed.[39] The possibilities of oxidative quenching and degradation of QDs in phagocytic cells have also been reported.[40] Fluorescent organosilica nanoparticles have stable fluorescence intensity in cells and may be more suitable to quantitative study of the interaction between nanoparticles and macrophages than QDs.

The TLFI and single-cell analysis revealed various patterns and kinetics of cellular uptake of macrophages after the dual administration of Flu-PEG30K and Rho. Flu-PEG30K showed a stealth effect, and many cells failed to take up Flu-PEG30K, including cells B1 and B2. These cells could be referred to as "PEG-sensitive macrophages". Some cells could take up Flu-PEG30K and showed various uptake patterns and kinetics. Cells B3 and B4 could take up Flu-PEG30K, but the uptake was lower than that of Rho. These cells could be referred to as "PEG-insensitive macrophages". PEG forms a flexible layer on the surface of the nanoparticles,[41] preventing the adsorption of proteins that act as opsonins[42,43] by blocking the protein-binding sites and creating a thermodynamic barrier against protein diffusion.[44−46] The PEGylation of nanoparticles can extend circulation half-life of particles. However, PEGylated nanoparticles are subsequently taken up by phagocytic cells such as macrophages.[47] The effects of size, shape, and surface chemistry of PEGylated particle against blood protein adsorption were investigated very well.[48−50] Recently, it was reported that time-dependent changes in the extracellular environment affected nanoparticle properties and their uptake by cells.[51] Cell B3 showed slow uptake after a lag phase of approximately 2 h. Some proteins may have been adsorbed with by the surface of Flu-PEG30K and increased during the lag phase; cell B3 may have started taking up the nanoparticles after this period. The loss of flexibility of the PEG layer due to protein adsorption and an expression and increase of membrane proteins that could bind to PEG (*i.e.*, a PEG receptor) during the lag phase may be another possibility.

There were some macrophages, such as cells B5 and B6, that took up PEGylated nanoparticles at the same level as Rho without any lag phase. These macrophages could be referred to as "PEG-resistant macrophages". The PEG-resistant macrophages and some PEG-insensitive macrophages (such as B4) do not have this uptake lag and should therefore have specific mechanisms, such as the expression of PEG receptor, for PEGylated nanoparticle uptake. Further studies are required to understand the association among PEG-insensitive macrophages, PEGylated nanoparticle, and adsorbed proteins. These results demonstrated that the stealth effect of PEG was dependent on each individual macrophage. Therefore, single-cell imaging, analysis, and characterization of the uptake kinetics of each macrophage are very important to understand the stealth effects of PEG.

Flow Cytometry Analysis of PEG-Resistant Macrophages. To statistically evaluate the existence of PEG-resistant macrophages, we performed FCM analysis using mouse peritoneal macrophages. Because the fluorescence of Rho could not be distinguished from that of Flu using FCM, we used Rub in place of Rho, as summarized in Figure 1B. The cells were treated with either no particles, Rub, Flu, a mixture of Rub and Flu, or a mixture of Rub and Flu-PEG30K and subjected to FCM. As shown in Figure 6A, the cells incubated with Flu or Rho show nanoparticle fluorescence of FL-1 for Flu (green dots) and FL-3 for Rub (red dots), respectively, and the cells without particles did not show obvious fluorescence under these experimental conditions (black dots). The profiles of Flu and Rub demonstrated no fluorescent crosstalk of the cells. The wide distribution of each fluorescence dot indicates that the nanoparticle uptake levels of the macrophages were heterogeneous. The results of the FCM were compatible with the results from the single-cell TLFI analysis. The cells treated with a mixture of Rub and Flu demonstrated a similar uptake of Rub and Flu because the cells showed a nearly linear relationship between the fluorescence of Flu and Rub (Figure 6B, orange dots). The FCM analysis of cells incubated with a mixture of Rub and Flu-PEG30K demonstrated that many cells took up Rub but not Flu-PEG30K (PEG-sensitive macrophages). Some cells could take up both Rub and Flu-PEG30K (*i.e.*, the PEG-insensitive macrophages) (Figure 6B, blue dots). Some blue dots were close to the linear distribution of the orange dots, indicating that the cells could take up both Rub and Flu-PEG30K at the same level; these cells are referred to as "PEG-resistant macrophages". In addition, the FCM analysis of cells incubated with a mixture of Rub and Flu-PEG12K also demonstrated the existence of many PEG-sensitive macrophages and some PEG-insensitive macrophages (Figure 6C, blue dots). These results indicated that PEG-resistant macrophages could take up PEGylated nanoparticles with a different PEG length. It has been reported that two kinds of liposomes PEGylated with PEG2K and PEG5K induced the ABC phenomena at the same level.[52] It is possible that PEG-resistant macrophages uptake the PEGylated particles without depending on PEG length and contribute ABC phenomenon *in vivo*.

The regional analysis of the FCM using Flu-PEG30K is summarized in Table 3 and Figure 6D. The cells took up both particles located in the upper right region. The population of the cells containing Rub and Flu-PEG30K located in upper right region (PEG-insensitive macrophages) were 3.3%. These results demonstrated that approximately 96.7% of mouse peritoneal macrophages could not take up Flu-PEG30K. As shown in Figure 6D, the percentage of macrophages that were insensitive to Flu-PEG30K was approximately 10 times lower than the percentage of macrophages

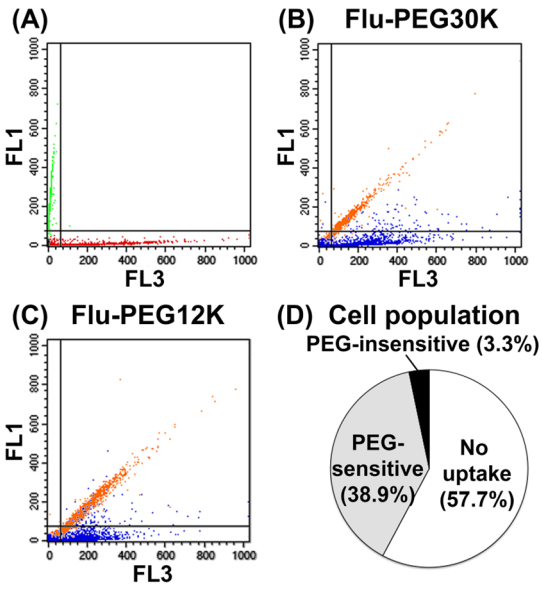

Figure 6. Flow cytometry analysis of macrophage uptake of dual fluorescent organosilica nanoparticles surface functionalized with PEG. The macrophages were incubated with either no particles, a single particle (Flu (green) or Rub (red)) (A), or two particles (a mixture of Flu and Rub (orange), a mixture of Flu-PEG30K and Rub (blue) (B) or Rub and Flu-PEG12K (blue dots) (C)); the macrophages were then analyzed by flow cytometry. (A) The cells without particles did not show obvious fluorescence and were located in the lower left region (black dots). The cells incubated with Flu or Rho show fluorescence of the nanoparticles in the FL1 channel (green dots) in the upper left region and the FL-3 channel in the lower right region (red dots), respectively. (B, C) The cells treated with a mixture of Rub and Flu (orange dots) showed fluorescence of both Rub and Flu in the upper right region. The cells incubated with a mixture of Rub and Flu-PEG30K (blue dots) (B) or Rub and Flu-PEG12K (blue dots) (C) showed mostly only fluorescence of Rub in the lower right region, but some cells showed fluorescence of both Rub and Flu-PEG30K in the upper right region. (D) The cell populations of no uptake, and PEG-sensitive and PEG-insensitive macrophage against Flu-PEG30K were graphed.

TABLE 3. Regional Analysis of Flow Cytometry in Macrophages after Dual Particle Administration

	lower left	lower right	upper left	upper right	*n* =
control	100.0	0.0	0.0	0.0	1
Flu	61.6 ± 18.7	0.0	38.4 ± 18.7	0.0	4
Rub	64.9 ± 4.7	35.1 ± 4.7	0.0	0.0	5
Rub + Flu	60.7 ± 10.3	5.9 ± 4.2	1.3 ± 1.6	32.1 ± 9.7	8
Rub + Flu-PEG30K	57.8 ± 11.8	38.9 ± 10.0	0.0	3.3 ± 4.4	10

that were sensitive to PEG. It has been previously reported that mushroom-type (0.028 ± 0.002 PEGs/nm^2) as well as brush-type 5K PEGylated PRINT nanoparticles (0.083 ± 0.006 PEGs/nm^2) were taken up 4−14 times less frequently than bare particles at early time points (0.5−6 h) by a mouse alveolar macrophage cell line (MH-S cells). The brush-type Flu-PEG30K revealed similar level of stealth functionality with respect to both mushroom-type and brush-type PEGylated PRINT nanoparticles.[53]

The standard deviations of the populations of the cells that took up both Rub and Flu-PEG30K were not very low, with values ranging from 0.2% (against 31.3% of uptake of Rub) to 14.4% (against 38.2% of uptake of Rub) (Table 3). These results indicated that the populations of PEG-insensitive macrophages may have individual differences and that some mice do not have many PEG-insensitive macrophages. It has been reported that ABC phenomena vary in different animal species.[21] It is possible that there are variations in responsiveness to PEGylated nanoparticles between species and individuals. A relationship between the population of PEG-insensitive macrophages and ABC phenomena may be important for understanding these individual species differences. It is possible that PEG-insensitive macrophages are an indicator of the ABC phenomenon. FCM analysis of the PEG-insensitive macrophages is possible for macrophages derived from the peritoneal cavity and from peripheral blood. Even for humans, the macrophage response to functionalized nanoparticles could be evaluated using macrophages from the peripheral blood. These approaches, including TLFI using simultaneous dual particle administration, could be useful for investigating the interactions between functionalized nanoparticles and individual macrophages and for developing personalized nanomedicine.

Characterization of PEG-Insensitive Macrophages. To characterize the PEG-insensitive macrophages, we performed correlative light and electron microscopy (CLEM), confocal laser scanning fluorescence microscopy, and cell surface marker analyses using FCM. To evaluate the morphological characteristics of the PEG-insensitive macrophages, we performed CLEM on the PEG-insensitive macrophages. As shown in Figure 7, scanning electron microscopy (SEM) using correlations with fluorescent microscopy (FM) identified the PEG-insensitive macrophages (marked with white arrowheads). The PEG-insensitive macrophages did not show specific morphological features or surface structures after TLFI compared to the cells with fluorescence derived from only Rho. It is well-known that the uptake of nanoparticles is mediated by phagocytosis, fluid-phase transport, or receptor-mediated endocytosis,[54−56] and these uptake routes are ultimately responsible for sequestering the particles in intracellular compartments, such as phagosomes, lysosomes, or endosomes. Other types of uptake, such as that mediated by surface-connected compartments (SCC) for hydrophobic nanoparticles and hydrophilic nanoparticles, have been reported to be important.[57] Further studies (such as CLEM) at various time points after the addition of nanoparticles and serial block-face SEM of cells are important for detecting the morphological characteristics of PEG-insensitive macrophages.

To evaluate the intracellular distribution of Rho and Flu-PEG30K in the PEG-insensitive macrophages, we performed confocal laser scanning fluorescence microscopy. As shown in Figure 8A, we observed three macrophages that were identified as PEG-insensitive PEG-sensitive cells (Figure 8C,D). The endosomes of the PEG-insensitive macrophages revealed various patterns of fluorescence (Figure 8B). The yellow arrowheads indicate that the endosomes contained almost equal amounts of Rho and Flu-PEG30K. We also observed endosomes that were predominantly either green or red fluorescent; these are indicated by the green and red arrowheads, respectively. The red endosomes contained more Rho than Flu-PEG30K (non-PEG dominant), and the green endosomes contained mostly Flu-PEG30K (PEG dominant). These results demonstrated that the endosomes have some selectivity for the surface properties of nanoparticles. Cell C showed one PEG-dominant endosome among many non-PEG-dominant endosomes. Cell D showed many non-PEG dominant endosomes, but not any obviously PEG-dominant endosomes. These results demonstrate that PEG-insensitive macrophages and some PEG-sensitive cells, such as cell C, could take up PEGylated nanoparticles and form PEG-dominant endosomes.

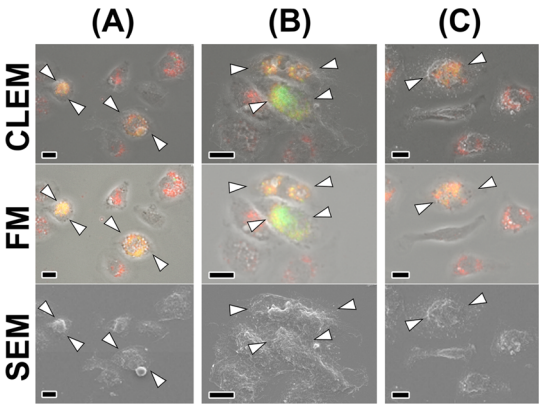

Figure 7. Correlative light and electron microscopy (CLEM) of the PEG-insensitive macrophages. (A−C) PEG-insensitive macrophages could be identified by scanning electron microscopy (SEM) using correlations with fluorescent microscopy (FM); these macrophages are marked with white arrow heads. The scale bars represent 10 μm.

These results are important for discussing the mechanism of PEG-sensitive, PEG-insensitive, and PEG-resistant macrophages. One hypothesis is that the macrophages have unique receptors for binding to PEGs. The PEG receptors bind with PEGylated nanoparticles to form PEG-dominant endosomes that can be distinguished from other receptors bound to bare nanoparticles. PEG-resistant macrophages might process PEG for antigen presentation.

Cell Surface Marker Analyses of PEG-Insensitive Macrophages Using Flow Cytometry. To investigate the specific cell surface markers of the PEG-insensitive macrophages, we performed FCM analyses using various cell surface markers for macrophages (Figure 9). The PEG-sensitive

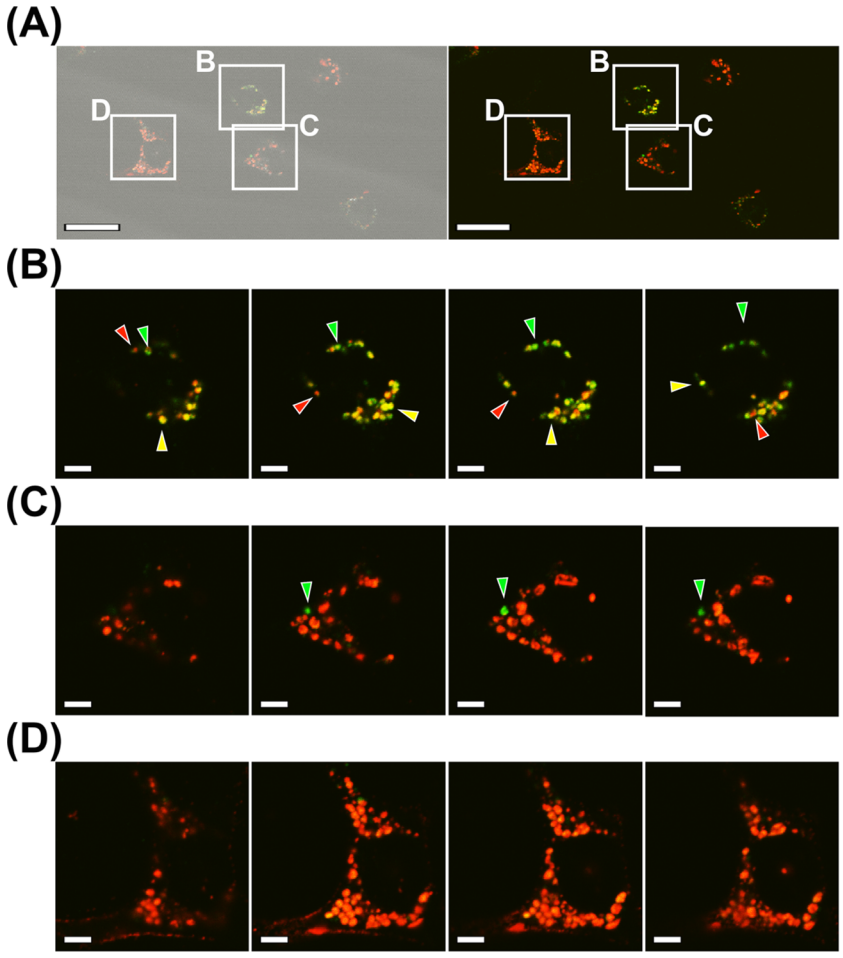

Figure 8. Confocal laser scanning fluorescence microscopy of the PEG-insensitive macrophages. (A) PEG-insensitive macrophage (B) and PEG-sensitive cells (C, D) were identified in merged fluorescent images. The scale bars represent 25 μm. (B−D) Cells were observed as cross sections at various *z*-axes to evaluate the intracellular distribution of Rho and Flu-PEG30K. (B) Endosomes of cell B revealed various patterns of fluorescence. The red, green, and yellow arrowheads indicate endosomes containing mainly Rho, Flu-PEG30K, and almost equal amounts of Rho and Flu-PEG30K, respectively. (C) Cell C showed one dominant endosome containing Flu-PEG30K, marked with a green arrow, among many endosomes containing Rho. (D) Cell D showed endosomes containing Rho and one endosome containing Flu-PEG30K. The scale bars represent 10 μm.

macrophages and PEG-insensitive macrophages are located under or above lines crossed in axis of FL1, respectively. Antibodies against CD209b (SIGN-R1), CD284 (TLR4), CD11b, CD282 (TLR2), F4/80, and CD36 reacted with the PEG-insensitive macrophages very well because of right shifts. Antibodies against CD11b, F4/80, CD205, CD11c, and CD36 reacted with the PEG-sensitive macrophages. The rates of increase in the fluorescence intensities of PEG-insensitive and PEG-sensitive macrophages and the increase in the ratio of PEG-insensitive to PEG-sensitive macrophages are provided in Table 4. Antibodies against CD209b showed a greater increase in fluorescence intensity in PEG-insensitive macrophages, and antibodies against CD11c and CD36 showed a lower increase in fluorescence intensity in PEG-insensitive macrophages. These results demonstrated that PEG-insensitive macrophages expressed more CD209b and less CD11c and CD36 among the peritoneal macrophage. CD209b would therefore be a possible PEG-insensitive macrophage marker. CD209b is a C-type lectin receptor (CLR) that is expressed at high levels in splenic marginal zone macrophages and lymph node medullary macrophages.[58] CLRs are particularly important pattern recognition receptors (PRRs) that recognize carbohydrate structure and take up glycosylated antigens and pathogens into cellular compartments. CD209b functions to take up dextran polysaccharides, including the capsular polysaccharide of *Streptococcus pneumoniae*.[59] PEGs have also repeated ethylene oxide units. It is possible that PEG-insensitive macrophages express PRRs against PEG as PEG receptors. Because the increase in the fluorescence intensity of CD209b on the PEG-insensitive macrophage relative to the PEG-sensitive macrophage was not very large, CD209b could not be the PEG receptor. However, it is possible that CD209b is associated with and coexpressed with the PEG receptor and contributes the uptake of PEGylated particle by macrophages. Isolation and further analysis using genomic and proteomic approaches in

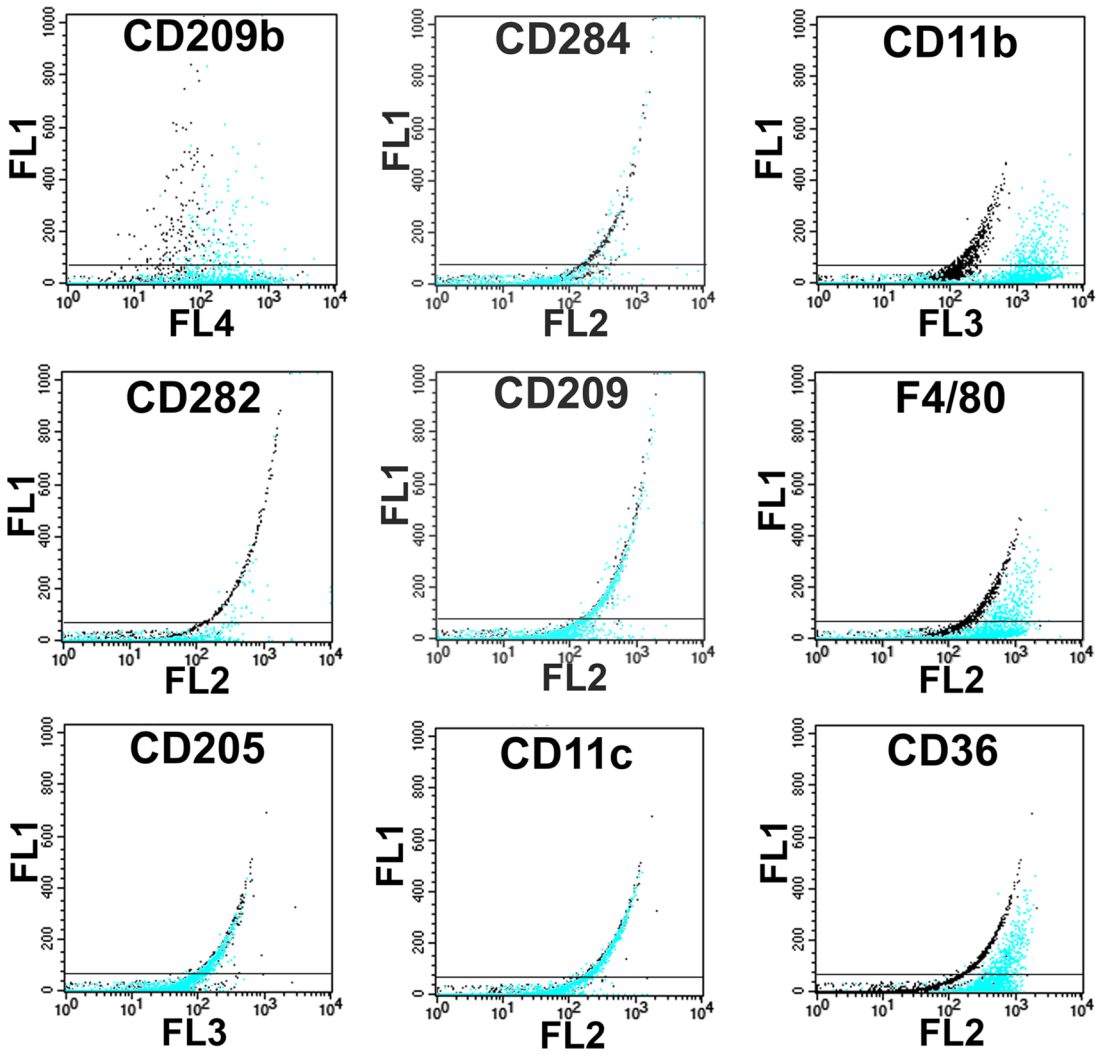

Figure 9. Cell surface marker analyses of the PEG-insensitive macrophages using flow cytometry. Various cell surface markers for macrophages were examined in the PEG-insensitive macrophages. Cells treated without and with antibodies are indicated by the black dots and light blue dots, respectively. PEG-sensitive macrophages and PEG-insensitive macrophages located below or above the line across the axis of FL1, respectively.

TABLE 4. Cell Surface Marker Analysis of PEG-Insensitive Macrophages

	antibody								
ratio	CD209b	CD284	CD11b	CD282	CD209	F4/80	CD205	CD11c	CD36
PEG-insensitive	5.97 ± 3.06	1.71 ± 0.45	7.25 ± 1.05	1.62 ± 1.31	1.10 ± 0.16	2.80 ± 0.67	1.37 ± 0.93	1.10 ± 0.16	4.43 ± 1.53
PEG-sensitive	1.69 ± 0.60	0.99 ± 0.28	5.64 ± 2.35	1.21 ± 0.91	1.51 ± 0.93	4.04 ± 1.23	2.13 ± 0.94	3.05 ± 0.66	25.73 ± 18.07
insensitive/sensitive	3.62 ± 1.34	1.92 ± 1.01	1.43 ± 0.15	1.31 ± 0.15	0.76 ± 0.21	0.70 ± 0.04	0.70 ± 0.21	0.37 ± 0.11	0.22 ± 0.10

PEG-insensitive macrophages would make it possible to identify the PEG receptor.

In this study, we investigated the interaction between mouse peritoneal macrophages and PEGylated nanoparticles using simultaneous dual organosilica particle administration, TLFI, single-cell analysis, and FCM. We identified PEG-insensitive macrophages, including PEG-resistant macrophages. The PEG-insensitive macrophages could take up PEGylated nanoparticles. Almost all of the macrophages failed to take up PEGylated nanoparticles, but we found PEG-insensitive macrophages using TLFI. The population of PEG-responsive macrophages was low and varied in individual mice. The PEG-insensitive macrophages showed various subclasses of endosomes, such as PEG-dominant and non-PEG-dominant endosomes. This is the first report describing variations in each macrophage's uptake of PEGylated nanoparticles *in vitro* and of PEG dominant endosomes in the cells. It is possible that the PEG-insensitive macrophages, especially the PEG-resistant

macrophages, play important roles in the immune responses against PEGylated nanoparticles, including the ABC phenomena. Macrophages play a scavenger role against "non-self" objects *in vivo* and act as the professional antigen-presenting dendritic cells.[60,61] Ishida *et al.* demonstrated that PEGylated liposomes were rapidly cleared from the blood circulation after repeated injections.[19−23,52,62−64] The accelerated blood clearance (ABC) of the second dose of PEGylated liposomes was caused by the binding of anti-PEG IgM, which is produced after the first dose of liposomes. The immunoresponse against PEGylated liposomes extends over a period of at least 2−3 days after the first injection. The anti-PEG IgM, produced by the splenic B cells that show T-cell independent (TI) immunity, could play a significant role in the induction of the ABC phenomenon. These patterns of IgM production are similar to the patterns found in splenic marginal zone (MZ) B cells and suggest the ability to produce large amounts of neutralizing antibodies.[65,66] MZ B cells play important roles in innate immunity and can rapidly produce antibodies in response to TI antigens, such as lipopolysaccharide (LPS) and polysaccharides. This TI immune response generates short-lived plasmablasts that secrete low-affinity IgM as early as 1−3 days after the exposure to blood-borne microorganisms.[67−69] The stimulation of MZ B cells against particulate TI antigens is regulated by various cells, such as circulating dendritic cells and MZ macrophages. The MZ macrophages capture antigens through various PRRs of the scavenger receptor and CLR families.[70,71] These PRRs bind to antigens with the help of complement and allow MZ macrophages to interact with TI antigens and present them to MZ B cells.[72−74] The TI antigens induce extensive cross-linking and coengagement between BCR on the MZ B cells and PRRs on the macrophages, and they stimulate MZ B cells.[71,74−76] TI antigen-interacting cells, including red pulp DCs and MZ macrophages, secrete interleukin-6 (IL-6), IL-10, type I interferons (IFNs), and CXC-chemokine ligand 10 (CXCL10), which cooperate with B cell activating factor (BAFF) and a proliferation-inducing ligand (APRIL) to promote the differentiation and survival of plasmablasts that secrete IgM.[71] In this study, we demonstrated the high expression of PRRs and CD209b (SIGN-R1) in PEG-resistant macrophages.

It has been reported that repeated injections of PEGylated liposomes containing doxorubicin did not induce the ABC phenomenon.[17] It is possible that PEG-resistant macrophages are associated with this phenomenon because PEG-resistant macrophages recognize PEGylated nanoparticles very well and would be in turn killed by cytotoxic drugs in liposomes. Further studies, such as the identification of PEG-resistant macrophages *in vivo*, especially in splenic marginal zone, and their characterizations such as the expression of the PRRs including CLR, and the presentation of PEG antigens, are required to understand the ABC phenomenon. The existence of PEG-resistant macrophages is new concept that may contribute to the understanding and regulation of immune responses against PEGylated nanoparticles. Identification and isolation of PEG-insensitive macrophages *in vitro* as well as *in vivo*, and further analysis using genomic and proteomic approaches would make it possible to find important molecules including the PEG receptor for the immunoresponse against PEG. Increasing the knowledge about PEG-resistant macrophages and their associated molecules, such as the PEG receptor and cytokines, would provide new strategies for innovative nanomedicine.

CONCLUSIONS

Stealth imaging using the simultaneous dual administration of two types of organosilica nanoparticles is useful for characterizing the behavior of individual macrophages with respect to PEGylated nanoparticles. The macrophage responsiveness to PEGylated nanoparticles was heterogeneous, and we observed a number of PEG-insensitive macrophages. We propose that PEG-insensitive macrophages, including PEG-resistant macrophages, are a new concept and that this concept is important for understanding and regulating the immune responses against PEGylated nanoparticles, such as the ABC phenomenon.

TLFI with single-cell analysis and FCM using simultaneous dual organosilica particle administration revealed a high potential for comparing two types of functional nanoparticles *in vitro*. Organosilica nanoparticles have increased biostability and functions compared with other functional nanoparticles, such as liposomes and polymers, because they do not degrade or release functional molecules such as fluorescent dyes. In addition to PEG, functional molecules for stealth function such as the "don't eat me" signal have been proposed and investigated.[77] Our approach would be useful in developing novel stealth nanoparticles based on the interactions between nanoparticles and immune cells.

MATERIALS AND METHODS

Materials. 3-Mercaptopropyltrimethoxysilane (MPMS), (3-Aminopropyl) trimethoxysilane (APS), fluorescein isothiocyanate isomer I, rhodamine B, and trisdichlororuthenium(II) hexahydrate were purchased from Sigma-Aldrich Chemical Co. (St. Louis, MO). Methoxy-PEG-maleimide [ME-300MA (M_w = 30000)] (PEG30K) and [ME-120MA (M_w = 12000)] (PEG12K) were purchased from the NOF Corp. (Tokyo, Japan). Ethyl alcohol and 28% NH_4OH were from the Katayama Chemical Co. (Osaka, Japan).

Preparation of Fluorescent Thiol−Organosilica Nanoparticles. Fluorescent thiol−organosilica nanoparticles containing rhodamine B (Rho) or trisdichlororuthenium(II) hexahydrate (Rub) were

prepared using a one-pot procedure as described previously.[22] In a typical synthesis, 10 screw-cap tubes containing 1035 μL of the reaction mixture (5 μL of 2 M MPMS, 30 μL of 100 mM rhodamine B, and 1000 μL of 28% NH_4OH in water) were mixed and incubated at 100 °C for 1 day. The nanoparticles containing fluorescein isothiocyanate (Flu) were prepared using APS–FITC conjugates. The conjugate was prepared by gentle stirring of a mixture of 250 mM APS and 250 mM fluorescein isothiocyanate for 1 h. The APS–FITC-conjugated solution was mixed with a mixture of 9 mM MPMS and 27% NH_4OH and incubated at 100 °C for 1 day. After incubation, the reaction mixture was subjected to centrifugation to remove the remaining reagents, and the pellets were sonicated and washed extensively with water 3 times. The pellets were dispersed in water. An aliquot of the particle solution was dried and weighed to determine the concentration of the particles.

Electron Microscopic Observation. For the nanoparticle evaluations, the particles were fixed on a 400-mesh copper grid coated with nitrocellulose and observed using a Hitachi H7650 transmission electron microscope (Hitachi, Tokyo, Japan). The diameters of a minimum of 100 particles were measured and calculated using Image-Pro Plus software (MediaCybernetics, Silver Spring, MD) to obtain the size distribution, mean diameter, and coefficients of variation (CVs).

Surface Functionalization of Fluorescent Thiol–Organosilica Nanoparticles with PEG. One milligram of Flu was mixed with 100 μL of 10 mM PEG30K or PEG12K, filled up to 1000 μL with distilled water, and incubated for 2 h at room temperature. After incubation, the mixture was centrifuged to remove the unbound reagent.

Dynamic Light Scattering and ζ Potential Analysis. Dynamic light scattering to analyze the size distributions and ζ potentials of nanoparticles was carried out with a NICOMP Submicron particle sizer, model 380/ZLS (Nicomp Particle Sizing Systems, Santa Barbara, CA) at room temperature. For the ζ potential analysis, the electrodes were dipped directly in the solution containing the silica nanoparticles. Based on the principles of electrophoretic light scattering, quantitative measures of the charge on the colloidal particles in liquid suspension were evaluated under the condition with E-field 5 V/cm, temperature 23 °C, viscosity 0.933 cP, reference index 1.333, dielectric constant 78.5, scattering angle 14.064°, and number-weighted Gaussian distribution analysis.

Thermal Gravimetric Analysis. The TGA of nanoparticles was performed using thermogravimetric/differential thermal analysis (TG-DTA, TG/DTA 6300, Siko Instruments Inc., Chiba, Japan). The data were obtained in flowing argon at a heating rate of 5 °C/min.

Fluorescence Microscopic Analysis. To evaluate the fluorescence intensity of single fluorescent organosilica nanoparticles on TLFI, the particles attached to the glass slide were imaged using a Nikon BioStation IM (Tokyo, Japan). The images were analyzed using Image-Pro Plus software as described previously.[34]

Time-Lapse Fluorescence Microscopic Imaging and Single-Cell Analysis of the Stealth Effect of PEG on Nanoparticles against Mouse Peritoneal Macrophages. ICR mouse peritoneal exudate cells were collected, and 1×10^5 cells were plated in 4 wells of a Hi-Q^4 multi-experiment dish (Ibidi GmbH, Munich, Germany). The nonadherent cells were removed by washing with RPMI 1640, and the macrophages were incubated in RPMI 1640 medium supplemented with 10% fetal bovine serum incubation at 37 °C for 24 h. The cells were treated with medium containing both Flu and Rho or both Flu-PEG30K and Rho (each particle concentration: 10 μg/mL) for the synchronized dual particle study. All of the media-containing particles were well suspended using sonication before their treatments to cells. The dish was placed into the live-imaging chamber of a Nikon BioStation IM. The acquired images were analyzed using Image-Pro Plus software.

Flow Cytometry Analysis. ICR mouse peritoneal exudate cells were collected, and 2×10^5 cells were plated on a 60 mm dish (Greiner Bio One, Frickenhausen, Germany). The nonadherent cells were removed by washing with RPMI 1640, and the macrophages were incubated in RPMI 1640 medium supplemented with 10% fetal bovine serum incubation at 37 °C for 24 h. The cells were treated with medium containing Flu, Rub, Flu and Rub, Flu-PEG30K and Rub, or Flu-PEG12K and Rub (each particle concentration: 10 μg/mL) for 6 h. All of the media-containing particles were well suspended using sonication before the treatments. The flow cytometry analysis was performed and analyzed using a FACSCalibur flow cytometer with Cell Quest software (Becton Dickinson, San Jose, CA). Fluorescence was detected on the FL1 channel (530/30 nm band-pass filter) and on the FL3 channel (670 nm long-pass filter).

To analyze the cell surface markers of the PEG-resistant macrophages, the cells treated with Rub-PEG30K were incubated with antimouse CD16/CD32 (Biolegend, CA, USA) at 4 °C for 10 min to block the Fc-receptor and then washed twice with cold buffer. The cells were then incubated with antimouse F4/80 antigen PE, antimouse CD209b (SIGN-R1) APC, CD11b PerCP-Cyanine5.5, antimouse CD11c PE, antimouse CD36 PE, antimouse CD205 PerCP-eFluor 710, antimouse CD209 (DC-SIGN) PE, antimouse CD282 (TLR2) PE, or antimouse CD284 (TLR4) PE from eBioscience (San Diego, CA) for 30 min at 4 °C and analyzed using a FACSCalibur flow cytometer.

Correlative Light and Electron Microscopic Observations of PEG-Insensitive Macrophages. For the morphological evaluation of PEG-insensitive macrophages, the macrophages incubated with Flu-PEG30K and Rho and observed on time-lapse fluorescence microscopic imaging were fixed with 2.5% glutaraldehyde, dehydrated in increased ethanol concentrations, dried by sublimation with *tert*-butyl alcohol by a vacuum pump, coated with 100% gold by an ion coater (Model IB-3, Eiko Engineering, Tokyo, Japan), and analyzed using a scanning electron microscope (JEOL JCM 5700, Tokyo, Japan). The images of the PEG-resistant macrophages on time-lapse fluorescence microscopic imaging and electron microscopy were analyzed and merged.

Confocal Microscopic Observation of PEG-Resistant Macrophages. The macrophages incubated with Flu-PEG30K and Rho were fixed with 4% paraformaldehyde, observed on a Nikon A1R laser scanning confocal microscope (equipped with CFI Plan Apo VC 60X WI objectives), and analyzed using NIS-Elements Software (Nikon, Tokyo, Japan).

Conflict of Interest: The authors declare no competing financial interest.

Acknowledgment. This work was supported in part by a Grant-in-Aid for Younger Scientists (No. 17790356) (to M.N.) and Grants-in-Aid for Scientific Research (C) (Nos. 19510117, 21500409, and 25350530) (to M.N.) from the Ministry of Education, Science, Sports, and Culture of Japan. This work was also supported by the Research for Promoting Technological Seeds and Adaptable and Seamless Technology Transfer Program through target-driven R&D from JST (AS2321114D) (to M.N.) and by a Grant for Practical Application of University R&D Results under the Matching Fund Method (to M.N.) from the New Energy and Industrial Technology Development Organization (NEDO) of Japan. We thank the Support Center for Advanced Medical Sciences, Institute of Health Biosciences, The University of Tokushima Graduate School, for their technical assistance.

Supporting Information Available: Dynamic light scattering analysis data of PEGylated Flu and bare fluorescent organosilica nanoparticles (Figure S1 and Table S1); movies of time-lapse fluorescent imaging of the macrophages incubated with Flu and Rho (movie S1) or with Flu-PEG30K and Rho (movie S2). This material is available free of charge *via* the Internet at http://pubs.acs.org.

REFERENCES AND NOTES

1. Moghimi, S. M.; Hunter, A. C.; Murray, J. C. Nanomedicine: Current Status and Future Prospects. *FASEB J.* **2005**, *19*, 311–330.
2. Liu, Y.; Miyoshi, H.; Nakamura, M. Nanomedicine for Drug Delivery and Imaging: A Promising Avenue for Cancer Therapy and Diagnosis Using Targeted Functional Nanoparticles. *Int. J. Cancer* **2007**, *120*, 2527–2537.
3. Liong, M.; Lu, J.; Kovochich, M.; Xia, T.; Ruehm, S. G.; Nel, A. E.; Tamanoi, F.; Zink, J. I. Multifunctional Inorganic

Nanoparticles for Imaging, Targeting, and Drug Delivery. *ACS Nano* **2008**, *2*, 889–896.
4. Namiki, Y.; Fuchigami, T.; Tada, N.; Kawamura, R.; Matsunuma, S.; Kitamoto, Y.; Nakagawa, M. Nanomedicine for Cancer: Lipid-Based Nanostructures for Drug Delivery and Monitoring. *Acc. Chem. Res.* **2011**, *44*, 1080–1093.
5. Tassa, C.; Shaw, S. Y.; Weissleder, R. Dextran-Coated Iron Oxide Nanoparticles: A Versatile Platform for Targeted Molecular Imaging, Molecular Diagnostics, and Therapy. *Acc. Chem. Res.* **2011**, *44*, 842–852.
6. Lee, J. E.; Lee, N.; Kim, T.; Kim, J.; Hyeon, T. Multifunctional Mesoporous Silica Nanocomposite Nanoparticles for Theranostic Applications. *Acc. Chem. Res.* **2011**, *44*, 893–902.
7. Khandare, J.; Calderón, M.; Dagia, N. M.; Haag, R. Multifunctional Dendritic Polymers in Nanomedicine: Opportunities and Challenges. *Chem. Soc. Rev.* **2012**, *41*, 2824–2848.
8. Yang, P.; Gai, S.; Lin, J. Functionalized Mesoporous Silica Materials for Controlled Drug Delivery. *Chem. Soc. Rev.* **2012**, *41*, 3679–3698.
9. Li, Z.; Barnes, J. C.; Bosoy, A.; Stoddart, J. F.; Zink, J. I. Mesoporous Silica Nanoparticles in Biomedical Applications. *Chem. Soc. Rev.* **2012**, *41*, 2590–2605.
10. Dreaden, E. C.; Alkilany, A. M.; Huang, X.; Murphy, C. J.; El-Sayed, M. A. The Golden Age: Gold Nanoparticles for Biomedicine. *Chem. Soc. Rev.* **2012**, *41*, 2740–2779.
11. Rosen, J. E.; Chan, L.; Shieh, D. B.; Gu, F. X. Iron Oxide Nanoparticles for Targeted Cancer Imaging and Diagnostics. *Nanomedicine* **2012**, *8*, 275–290.
12. Doane, T. L.; Burda, C. The Unique Role of Nanoparticles in Nanomedicine: Imaging, Drug Delivery and Therapy. *Chem. Soc. Rev.* **2012**, *41*, 2885–2911.
13. Matsumura, Y.; Maeda, H. A New Concept for Macromolecular Therapeutics in Cancer Chemotherapy: Mechanism of Tumoritropic Accumulation of Proteins and the Antitumor Agent Smancs. *Cancer Res.* **1986**, *46*, 6387–6392.
14. Maeda, H.; Matsumura, Y. Tumoritropic and Lymphotropic Principles of Macromolecular Drugs. *Crit. Rev. Ther. Drug Carrier Syst.* **1989**, *6*, 193–210.
15. Fang, J.; Nakamura, H.; Maeda, H. The EPR effect: Unique Features of Tumor Blood Vessels for Drug Delivery, Factors Involved, and Limitations and Augmentation of the Effect. *Adv. Drug Delivery Rev.* **2011**, *63*, 136–151.
16. Moghimi, S. M.; Hunter, A. C.; Murray, J. C. Long-Circulating and Target-Specific Nanoparticles: Theory to Practice. *Pharmacol. Rev.* **2001**, *53*, 283–318.
17. Dams, E. T.; Laverman, P.; Oyen, W. J.; Storm, G.; Scherphof, G. L.; van Der Meer, J. W.; Corstens, F. H.; Boerman, O. C. Accelerated Blood Clearance and Altered Biodistribution of Repeated Injections of Sterically Stabilized Liposomes. *J. Pharmacol. Exp. Ther.* **2000**, *29*, 1071–1079.
18. Laverman, P.; Carstens, M. G.; Boerman, O. C.; Dams, E. T.; Oyen, W. J.; van Rooijen, N.; Corstens, F. H.; Storm, G. Factors Affecting the Accelerated Blood Clearance of Polyethylene Glycol-Liposomes Upon Repeated Injection. *J. Pharmacol. Exp. Ther.* **2001**, *298*, 607–612.
19. Ishida, T.; Maeda, R.; Ichihara, M.; Mukai, Y.; Motoki, Y.; Manabe, Y.; Irimura, K.; Kiwada, H. The Accelerated Clearance on Repeated Injection of PEGylated Liposomes in Rats: Laboratory and Histopathological Study. *Cell. Mol. Biol. Lett.* **2002**, *7*, 286.
20. Ishida, T.; Maeda, R.; Ichihara, M.; Irimura, K.; Kiwada, H. Accelerated Clearance of PEGylated Liposomes in Rats After Repeated Injections. *J. Controlled Release* **2003**, *88*, 35–42.
21. Abu Lila, A. S.; Kiwada, H.; Ishida, T. The Accelerated Blood Clearance (ABC) Phenomenon: Clinical Challenge and Approaches to Manage. *J. Controlled Release* **2013**, *172*, 38–47.
22. Ishida, T.; Wang, X.; Shimizu, T.; Nawata, K.; Kiwada, H. PEGylated Liposomes Elicit an Anti-PEG IgM Response in a T Cell-Independent Manner. *J. Controlled Release* **2007**, *122*, 349–355.
23. Wang, X.; Ishida, T.; Kiwada, H. Anti-PEG IgM Elicited By Injection of Liposomes Is Involved in the Enhanced Blood Clearance of a Subsequent Dose of PEGylated Liposomes. *J. Controlled Release* **2007**, *119*, 236–244.
24. Nakamura, M.; Ishimura, K. Synthesis and Characterization of Organosilica Nanoparticles Prepared from 3-Mercaptopropyltrimethoxysilane as the Single Silica Source. *J. Phys. Chem. C* **2007**, *111*, 18892–18898.
25. Nakamura, M.; Ishimura, K. One-Pot Synthesis and Characterization of Three Kinds of Thiol-Organosilica Nanoparticles. *Langmuir* **2008**, *24*, 5099–5108.
26. Nakamura, M.; Ishimura, K. Size-Controlled, One-Pot Synthesis, Characterization, and Biological Applications of Epoxy-Organosilica Particles Possessing Positive Zeta Potential as Prepared. *Langmuir* **2008**, *24*, 12228–12234.
27. Nakamura, M. *Nanostructured Oxides*; Wiley-VCH: Weinheim, 2009; pp 109−161.
28. Nakamura, M.; Ozaki, S.; Abe, M.; Doi, H.; Matsumoto, T.; Ishimura, K. One-pot Synthesis, Characterization, and Biological Applications of Size-Controlled Thiol-Organosilica Nanoparticles Prepared from 3-Mercaptopropyltrimethoxysilane. *Colloids Surf. B: Biointerfaces* **2010**, *79*, 19–26.
29. Nakamura, M.; Ozaki, S.; Abe, M.; Matsumoto, T.; Ishimura, K. One-pot synthesis and Characterization of Dual Fluorescent Thiol-Organosilica Nanoparticles as Non-Photoblinking Quantum Dots and Their Applications for Biological Imaging. *J. Mater. Chem.* **2011**, *21*, 4689–4695.
30. Nakamura, M.; Awaad, A.; Hayashi, K.; Ochiai, K.; Ishimura, K. Thiol-organosilica Particles Internally Functionalized with Propidium Iodide as a Multicolor Fluorescence and X-Ray Computed Tomography Probe and Application for Non-Invasive Functional Gastrointestinal Tract Imaging. *Chem. Mater.* **2012**, *24*, 3772–3779.
31. Nakamura, M. Biomedical Applications of Organosilica Nanoparticles Toward Theranostics. *Nanotechnol. Rev.* **2012**, *1*, 469–491.
32. Awaad, A.; Nakamura, M.; Ishimura, K. Imaging of Size Dependent Uptake and Identification of Novel Pathway in Mouse Peyer's Patches Using Fluorescent Organosilica Particles. *Nanomed.: NBM* **2012**, *8*, 627–636.
33. Awaad, A.; Nakamura, M.; Ishimura, K. Histochemical and Biochemical Analysis of the Size-Dependent Nanoimmunoresponse in Mouse Peyer's Patches Using Fluorescent Organosilica Particles. *Int. J. Nanomed.* **2012**, *7*, 1423–1439.
34. Nakamura, M.; Miyamoto, K.; Hayashi, K.; Awaad, A.; Ochiai, M.; Ishimura, K. Time-Lapse Fluorescence Imaging and Quantitative Single Cell and Endosomal Analysis of Peritoneal Macrophages Using Fluorescent Organosilica Nanoparticles. *Nanomed.: NBM* **2013**, *9*, 274–283.
35. Nakamura, M.; Ishimura, K. Rapid Size Evaluation of Nanoparticles Using Flow Cytometry. *Adv. Sci. Lett.* **2010**, *3*, 130–137.
36. Tirosh, O.; Barenholz, Y.; Katzhendler, J.; Priev, A. Hydration of Polyethylene Glycol-Grafted Liposomes. *Biophys. J.* **1998**, *74*, 1371–1379.
37. Gref, R.; Lück, M.; Quellec, P.; Marchand, M.; Dellacherie, E.; Harnisch, S.; Blunk, T.; Müller, R. H. 'Stealth' Corona-Core Nanoparticles Surface Modified By Polyethylene Glycol (PEG): Influences of the Corona (PEG Chain Length and Surface Density) and of the Core Composition on Phagocytic Uptake and Plasma Protein Adsorption. *Colloids Surf. B: Biointerfaces* **2000**, *18*, 301–313.
38. Medintz, I. L.; Uyeda, H. T.; Goldman, E. R.; Mattoussi, H. Quantum Dot Bioconjugates for Imaging, Labelling and Sensing. *Nat. Mater.* **2005**, *4*, 435–446.
39. Hanaki, K.; Momo, A.; Oku, T.; Komoto, A.; Maenosono, S.; Yamaguchi, Y.; Yamamoto, K. Semiconductor Quantum Dot/Albumin Complex Is a Long-life and Highly Photostable Endosome Marker. *Biochem. Biophys. Res. Commun.* **2003**, *302*, 496–501.
40. Mancini, M. C.; Kairdolf, B. A.; Smith, A. M.; Nie, S. Oxidative Quenching and Degradation of Polymer-Encapsulated Quantum Dots: New Insights into The Long-Term Fate and Toxicity Of Nanocrystals *In Vivo*. *J. Am. Chem. Soc.* **2008**, *130*, 10836–10837.

41. Heald, C. R.; Stolnik, S.; Kujawinski, K. S.; De Matteis, C.; Garnett, M. C.; Illum, L.; Davis, S. S.; Purkiss, S. C.; Barlow, R. J.; Gellert, P. R. Poly(Lactic Acid)-Poly(Ethylene Oxide) (PLA-PEG) Nanoparticles: NMR Studies of the Central Solid Like PLA Core and the Liquid PEG Corona. *Langmuir* **2002**, *18*, 3669–3675.
42. Moffatt, S.; Cristiano, R. J. Uptake Characteristics of NGR-Coupled Stealth PEI/PDNA Nanoparticles Loaded with PLGA-PEG-PLGA Tri-Block Copolymer for Targeted Delivery to Human Monocyte- Derived Dendritic Cells. *Int. J. Pharm.* **2006**, *321*, 143–154.
43. Kenausis, G. L.; Vörös, J.; Elbert, D. L.; Huang, N.; Hofer, R.; Ruiz-Taylor, L.; Textor, M.; Hubbell, J. A.; Spencer, N. D. Poly(l-lysine)-g-Poly(ethylene glycol) Layers on Metal Oxide Surfaces: Attachment Mechanism and Effects of Polymer Architecture on Resistance to Protein Adsorption. *J. Phys. Chem. B* **2000**, *104*, 3298–3309.
44. Szleifer, I. Protein Adsorption on Surfaces with Grafted Polymers: A Theoretical Approach. *Biophys. J.* **1997**, *72*, 595–612.
45. Jeon, S. I.; Lee, J. H.; Andrade, J. D.; De Gennes, P. G. Protein—Surface Interactions in The Presence of Polyethylene Oxide: I. Simplified Theory. *J. Colloid Interface Sci.* **1991**, *142*, 149–158.
46. Satulovsky, J.; Carignano, M. A.; Szleifer, I. Kinetic and Thermodynamic Control of Protein Adsorption. *Proc. Natl. Acad. Sci. U.S.A.* **2000**, *97*, 9037–9041.
47. Storm, G.; Belliot, S. O.; Daemen, T.; Lasic, D. D. Surface Modification of Nanoparticles to Oppose Uptake By the Mononuclear Phagocyte System. *Adv. Drug Delivery Rev.* **1995**, *17*, 31–48.
48. Mu, Q.; Li, Z.; Li, X.; Mishra, S. R.; Zhang, B.; Si, Z.; Yan, B. Characterization of Protein Clusters of Diverse Magnetic Nanoparticles and Their Dynamic Interactions with Human Cells. *J. Phys. Chem. C* **2009**, *113*, 5390–5395.
49. Walkey, C. D.; Olsen, J. B.; Guo, H.; Emili, A.; Chan, W. C. Nanoparticle Size and Surface Chemistry Determine Serum Protein Adsorption and Macrophage Uptake. *J. Am. Chem. Soc.* **2012**, *134*, 2139–2147.
50. Benetti, F.; Fedel, M.; Minati, L.; Speranza, G.; Migliaresi, C. Gold Nanoparticles: Role of Size and Surface Chemistry on Blood Protein Adsorption. *J. Nanopart. Res.* **2013**, *15*, 1–9.
51. Albanese, A.; Walkey, C. D.; Olsen, J. B.; Guo, H.; Emili, A.; Chan, W. C. Secreted Biomolecules Alter the Biological Identity and Cellular Interactions of Nanoparticles. *ACS Nano* **2014**, *8*, 5515–5526.
52. Ishida, T.; Harada, M.; Wang, X. Y.; Ichihara, M.; Irimura, K.; Kiwada, H. Accelerated Blood Clearance of PEGylated Liposomes Following Preceding Liposome Injection: Effects of Lipid Dose and PEG Surface-Density and Chain Length of the First-Dose Liposomes. *J. Controlled Release* **2005**, *105*, 305–317.
53. Perry, J. L.; Reuter, K. G.; Kai, M. P.; Herlihy, K. P.; Jones, S. W.; Luft, J. C.; Napier, M.; Bear, J. E.; DeSimone, J. M. PEGylated PRINT Nanoparticles: The Impact of PEG Density on Protein Binding, Macrophage Association, Biodistribution, and Pharmacokinetics. *Nano Lett.* **2012**, *12*, 5304–5310.
54. Rejman, J.; Oberle, V.; Zuhorn, I. S.; Hoekstra, D. Size-Dependent Internalization of Particles *via* the Pathways of Clathrin-and Caveolae-Mediated Endocytosis. *Biochem. J.* **2004**, *377*, 159–169.
55. Mohanraj, V. J.; Chen, Y. Nanoparticles-A Review. *Trop. J. Pharm. Res.* **2006**, *5*, 561–573.
56. Chithrani, B. D.; Ghazani, A. A.; Chan, W. C. Determining the Size and Shape Dependence of Gold Nanoparticle Uptake into Mammalian Cells. *Nano Lett.* **2006**, *6*, 662–668.
57. Motskin, M.; Müller, K. H.; Genoud, C.; Monteith, A. G.; Skepper, J. N. The Sequestration of Hydroxyapatite Nanoparticles by Human Monocyte-Macrophages in a Compartment that Allows Free Diffusion with the Extracellular Environment. *Biomaterials* **2011**, *32*, 9470–9482.
58. Kang, Y. S.; Yamazaki, S.; Iyoda, T.; Pack, M.; Bruening, S. A.; Kim, J. Y.; Takahara, K.; Inaba, K.; Steinman, R. M.; Park, C. G. SIGN-R1, A Novel C-Type Lectin Expressed by Marginal Zone Macrophages in Spleen, Mediates Uptake of the Polysaccharide Dextran. *Int. Immunol.* **2003**, *15*, 177–186.
59. Kang, Y. S.; Kim, J. Y.; Bruening, S. A.; Pack, M.; Charalambous, A.; Pritsker, A.; Moran, T. M.; Loeffler, J. M.; Steinman, R. M.; Park, C. G. The C-Type Lectin SIGN-R1Mediates Uptake of the Capsular Polysaccharide of *Streptococcus Pneumoniae* in the Marginal Zone of Mouse Spleen. *Proc. Natl. Acad. Sci. U.S.A.* **2004**, *101*, 215–220.
60. Aderem, A.; Underhill, D. M. Mechanisms of Phagocytosis in Macrophages. *Annu. Rev. Immunol.* **1999**, *17*, 593–623.
61. Greaves, D. R.; Gordon, S. The Macrophage Scavenger Receptor at 30 Years of Age: Current Knowledge and Future challenges. *J. Lipid Res.* **2009**, *50*, S282–286.
62. Ishida, T.; Ichihara, M.; Wang, X.; Yamamoto, K.; Kimura, J.; Majima, E.; Kiwada, H. Injection of PEGylated Liposomes in Rats Elicits PEG-Specific IgM, Which Is Responsible for Rapid Elimination of a Second Dose of PEGylated Liposomes. *J. Controlled Release* **2006**, *112*, 15–25.
63. Ishida, T.; Masuda, K.; Ichikawa, T.; Ichihara, M.; Irimura, K.; Kiwada, H. Accelerated Clearance of a Second Injection of PEGylated Liposomes in Mice. *Int. J. Pharm.* **2003**, *255*, 167–174.
64. Dams, E. T. M.; Laverman, P.; Oyen, W.J. G.; Storm, G.; Scherphof, G. L.; van der Meer, J. W. M.; Corstens, F. H. M.; Boerman, O. C. Accelerated Blood Clearance and Altered Biodistribution of Repeated Injections of Sterically Stabilized Liposomes. *J. Pharmacol. Exp. Ther.* **2000**, *292*, 1071–1079.
65. Martin, F.; Oliver, A. M.; Kearney, J. F. Marginal Zone and B1 B Cells Unite in the Early Response Against T-Independent Blood-Borne Particulate Antigens. *Immunity* **2001**, *14*, 617–629.
66. Zandvoort, A.; Timens, W. The Dual Function of the Splenic Marginal Zone: Essential for Initiation of Anti-TI-2 Responses but also Vital in the General First-Line Defense Against Blood-Borne Antigens. *Clin. Exp. Immunol.* **2002**, *130*, 4–11.
67. Martin, F.; Oliver, A. M.; Kearney, J. F. Marginal Zone and B1 B Cells Unite in the Early Response Against T-Independent Blood-Borne Particulate Antigens. *Immunity* **2001**, *14*, 617–629.
68. Colino, J.; Shen, Y.; Snapper, C. M. Dendritic Cells Pulsed with Intact Streptococcus Pneumoniae Elicit Both Prowtein- and Polysaccharide-Specific Immunoglobulin Isotype Responses *In Vivo* Through Distinct Mechanisms. *J. Exp. Med.* **2002**, *195*, 1–13.
69. Do, R. K.; Hatada, E.; Lee, H.; Tourigny, M. R.; Hilbert, D.; Chen-Kiang, S. Attenuation of Apoptosis Underlies B Lymphocyte Stimulator Enhancement of Humoral Immune Response. *J. Exp. Med.* **2002**, *192*, 953–964.
70. Chen, Y.; Pikkarainen, T.; Elomaa, O.; Soininen, R.; Kodama, T.; Kraal, G.; Tryggvason, K. Defective Microarchitecture of the Spleen Marginal Zone and Impaired Response to a Thymus-Independent Type 2 Antigen in Mice Lacking Scavenger Receptors MARCO and SR-A. *J. Immunol.* **2005**, *175*, 8173–8180.
71. Kang, Y. S.; Do, Y.; Lee, H. K.; Park, S. H.; Cheong, C.; Lynch, R. M.; Loeffler, J. M.; Steinman, R. M.; Park, C. G. A Dominant Complement Fixation Pathway for Pneumococcal Polysaccharides Initiated By SIGN-R1 Interacting with C1q. *Cell* **2006**, *125*, 47–58.
72. Mond, J. J.; Lees, A.; Snapper, C. M. T Cell-Independent Antigens Type 2. *Annu. Rev. Immunol.* **1995**, *13*, 655–692.
73. Mebius, R. E.; Kraal, G. Structure and Function of the Spleen. *Nature Rev. Immunol.* **2005**, *5*, 606–616.
74. Pone, E. J.; Zhang, J.; Mai, T.; White, C. A.; Li, G.; Sakakura, J. K.; Patel, P. J.; Al-Qahtani, A.; Zan, H.; Xu, Z.; Casali, P. BCR-Signalling Synergizes with TLR- Signalling for Induction of AID and Immunoglobulin Class-Switching Through the Non-Canonical NF-KB Pathway. *Nature Commun.* **2012**, *3*, 767.
75. Mond, J. J.; Lees, A.; Snapper, C. M. T cell-independent antigens type 2. *Annu. Rev. Immunol.* **1995**, *13*, 655–692.

76. Bergtold, A.; Desai, D. D.; Gavhane, A.; Clynes, R. Cell surface recycling of internalized antigen permits dendritic cell priming of B cells. *Immunity* **2005**, *23*, 503–514.
77. Rodriguez, P. L.; Harada, T.; Christian, D. A.; Pantano, D. A.; Tsai, R. K.; Discher, D. E. Minimal "Self" Peptides That Inhibit Phagocytic Clearance and Enhance Delivery of Nanoparticles. *Science* **2013**, *339*, 971–975.